JOURNAL OF SOLID STATE CHEMISTRY 69, 162–170 (1987)

Structure Systematics in $A_3Mo_2X_9$, X = Cl, Br, I, from Rietveld Refinement of X-ray Powder Data

ROBERT STRANGER,* IAN E. GREY,† IAN C. MADSEN,† AND PETER W. SMITH*

Chemistry Department, University of Tasmania, P.O. Box 252 C, Hobart, Tasmania 7001, and †CSIRO Division of Mineral Chemistry, P.O. Box 124, Port Melbourne, Victoria 3207, Australia

Received October 8, 1986

The structures of the compounds $A_3Mo_2Cl_9$, A = K, NH_4, Rb, Cs, Me_4N; $A_3Mo_2Br_9$, A = K, Rb, Cs, Me_4N; $Cs_3Mo_2I_9$, and $Cs_3W_2Cl_9$ have been refined by Rietveld analysis of powder X-ray diffraction data. The results have been used to analyze the effect of change of the A cation on the geometry of the $(M_2X_9)^{3-}$ complex anion, which comprises two octahedra sharing a common face. The observed increase in the M–M separation with increasing size of the A cation is interpreted in terms of a balance between attractive M–M bonding forces, which draw the metals together, and strong covalent M-terminal halogen bonds which, together with elongation of $(M_2X_9)^{3-}$ due to packing effects, cause a net lengthening of M–M. In the series $A_3Mo_2Cl_9$, for example, the Mo–Mo separation increases from 2.524(8) to 2.778(8) Å when the A cation changes from K to Me_4N.

Introduction

The enneahalodimetalates, $A_3M_2X_9$, of trivalent Cr, Mo, and W form an interesting class of compounds for the study of magnetic interactions (*1*). The compounds contain isolated binuclear complex anions, $(M_2X_9)^{3-}$, formed by two octahedra sharing a face, and magnetic interactions can occur by direct exchange due to overlap of metal orbits and by super exchange via the bridging halogen atoms. In $K_3W_2Cl_9$ strong metal–metal bonding occurs, resulting in a very short W–W separation of 2.41 Å (*2*) and paired-electron, temperature-independent magnetic behavior. In contrast, $Cs_3Cr_2Cl_9$ has a long Cr–Cr separation of 3.12 Å (*3*), corresponding to a net repulsion of the Cr atoms, and the magnetic exchange is very weak.

The corresponding molybdenum compounds display intermediate bonding and magnetic behavior. The reported Mo–Mo separation in $Cs_3Mo_2Cl_9$ is 2.66 Å (*4*), which represents a small net attraction of the Mo atoms towards each other. The electronic spectra for $A_3Mo_2X_9$ can be interpreted in terms of a model in which one d electron per Mo is paired in a σ-bond, and the other two d electrons per Mo are involved in weaker π-interactions (*5*). From magnetic measurements on series of chloride and bromide compounds, we have previously determined the magnetic exchange integral, $-J$, and have attempted to relate the exchange to the variation in Mo–Mo separation (*1*). The latter was calculated from the unit cell parameters for different $A_3Mo_2X_9$ by assuming that the fractional coordinates for Mo remained unchanged at

0022-4596/87 $3.00

the values for the cesium compound (*6*). The plot of $-J$ versus Mo–Mo showed an exponential form, with increasing Mo–Mo separation related to increasing A cation size in the series with A = K, Cs, Me_4N, and Et_4N.

Recent single-crystal refinements and magnetic measurements have been reported for enneachlorodimolybdates with pyridinium and piperidinium cations (*7*). The resulting values of $-J$ and Mo–Mo did not lie on our previously determined curve, and this raised doubts on the validity of our assumption of transferable Mo atomic coordinates to large A cations in the $A_3Mo_2X_9$ series. Structural data had not previously been available for compounds with a range of A cations because of the difficulty in growing single crystals. However, with the development of the Rietveld profile refinement method (*8*), accurate structural parameters can now be routinely obtained by refinement of powder data. We report here the results of Rietveld refinement of powder X-ray diffraction data for the compounds $A_3Mo_2Cl_9$, A = K, NH_4, Rb, Cs, Me_4N; $A_3Mo_2Br_9$, A = K, Rb, Cs, Me_4N; and $Cs_3Mo_2I_9$, as well as the tungsten compound $Cs_3W_2Cl_9$.

Experimental

The preparation methods for the alkali and alkyl ammonium salts of $M_2X_9^{3-}$ have been previously reported (*9, 10*).

Step-scan X-ray powder intensity data were obtained at 24°C with a Philips PW1050 goniometer/PW1710 controller. Intensity measurements in the range 7 to 90°, 2θ, were made at intervals of 0.04°, using CuK_α radiation and a step-counting time of 5 sec. The X-ray tube was operated at 45 kV and 30 mA, with a 1° divergence slit, a 0.2-mm receiving slit, a 1° scatter slit and soller slits. For angles less than 14°, 2θ, a geometrical correction was made for the spread of the beam beyond the specimen.

The reported atomic coordinates for $Cs_3Mo_2Cl_9$, given in Table I, were used to initiate refinement, in $P6_3/mmc$, of the data for all compounds except the potassium salts. These were refined in $P6_3/m$, using the reported coordinates for $K_3W_2Cl_9$ (*2*) as starting values. Least-squares structure refinements were carried out with the Rietveld analysis program DBW 3.2 (*11*), which has been modified to include of 2θ-variable pseudo-Voigt peak shape function (*12*). The method of extraction of "observed" integrated peak intensities for the calculation of Fourier coefficients and Bragg agreement indices has also been improved. Profile refinement parameters included a scale factor, two pseudo-Voigt shape parameters, a 2θ zero parameter, a peak full-width at half-maximum (FWHM) function of the form $FWHM^2 = U\tan^2\theta + V\tan\theta + W$, when U, V, and W are refinable parameters (*13*), calculated for 5.0 half-widths on either side of the peak maximum, a peak asymmetry parameter (*8*) for reflections with $d > 2.2$ Å, and the unit cell parameters. For some refinements of the data for $Cs_3Mo_2Cl_9$, the background was evaluated by linear interpolation between measured points distributed over the whole pattern. All other refinements included a refinement of the background using a six-parameter polynomial in $2\theta^n$, where n has values from -1 to 4 inclusive. An experimentally determined value of 0.91 was used for the monochromator polarization correction (*14*).

TABLE I

STRUCTURE DATA FOR $Cs_3Mo_2Cl_9$ FROM REFERENCE (*4*)[a]

Atom	Site	Point symmetry	x	y	z
Cs(1)	2(*b*)	$\bar{6}m2$	0	0	$\frac{1}{4}$
Cs(2)	4(*f*)	3*m*	$\frac{1}{3}$	$\frac{2}{3}$	0.0743(2)
Mo	4(*f*)	3*m*	$\frac{1}{3}$	$\frac{2}{3}$	0.8257(3)
Cl(1)	6(*h*)	*mm*	0.5016(11)	1.0032	$\frac{1}{4}$
Cl(2)	12(*k*)	*m*	0.8208(8)	1.6415	0.0973(5)

[a] a = 7.357(5), c = 17.545(12) Å.

Neutral atom X-ray scattering factors, including anomalous dispersion corrections, were taken from "International Tables for X-Ray Crystallography" (*15*).

Results and Discussion

1. Precision and Accuracy of Refinements

For the compound $Cs_3Mo_2Cl_9$, five separate Rietveld refinements were carried out to test the precision with which the parameters could be reproduced and their accuracy relative to the published parameters from a single-crystal refinement (*4*). The refined parameters included the profile parameters described under Experimental, coordinates, and anisotropic thermal parameters. Convergence was considered to be achieved when the parameter shifts were less than 25% of the associated esd's. The refined cell parameters and coordinates are given in Table II. Thermal parameters and lists of step intensity data may be obtained from the authors. The observed, calculated, and difference diffraction profiles for one of the samples (run E in Table II) is given in Fig. 1.

Runs A to C correspond to separate packings and data collections for the same sample. The data collection and refinement conditions were the same for these three samples. The precision in the refined parameters is excellent. The coordinates from the three refinements agree within one combined Rietveld esd and the cell parameters agree within two combined esd's. Run D was made using the same sample and differs only in that the background was refined rather than determined from interpolation between measured values. Both the weighted profile R factor and the Bragg R factor are much lower for run D than for the first three runs. However, some of the refined parameters differ considerably. The final refinement, run E, was carried out on a different sample, of higher crystallinity (FWHM at 40° (2θ) = 0.16° compared with 0.40° for the first sample). A scatter slit was used in the data collection for this sample, which considerably improved the peak-to-background ratio, especially at the lower angles. The narrower peaks for this sample were more difficult to fit, as illustrated by the higher value of R_{wp} in Table II, although the structure refinement was very good, with R_B = 3.15%.

The average parameter values from the

TABLE II

RIETVELD REFINEMENT DATA FOR $Cs_3Mo_2Cl_9$

	Run A[a]	Run B[a]	Run C[a]	Run D[b]	Run E[c]	Average
a (Å)	7.3300(5)	7.3281(4)	7.3298(5)	7.3255(4)	7.3395(2)	7.330(5)
c (Å)	17.518(1)	17.516(1)	17.520(1)	17.513(1)	17.4997(6)	17.513(8)
z (Mo)	0.8265(2)	0.8264(2)	0.8262(2)	0.8256(1)	0.8263(2)	0.8262(3)
z (Cs(2))	0.0745(2)	0.0745(2)	0.0745(2)	0.0752(1)	0.0740(1)	0.0745(3)
x (Cl(1))	0.4995(5)	0.5004(5)	0.5006(5)	0.5042(4)	0.4995(5)	0.501(2)
x (Cl(2))	0.8246(4)	0.8242(4)	0.8241(4)	0.8187(3)	0.8254(4)	0.823(3)
z (Cl(2))	0.0948(2)	0.0946(2)	0.0950(2)	0.0957(2)	0.0976(2)	0.096(1)
R_{wp} (%)	6.43	6.22	6.30	4.22	10.13	
R_B (%)	7.33	5.43	5.59	1.50	3.15	

[a] Interpolated backgrounds, no scatter slit.
[b] Same sample as a, refined backgrounds, no scatter slit.
[c] New sample, refined background, scatter slit used.

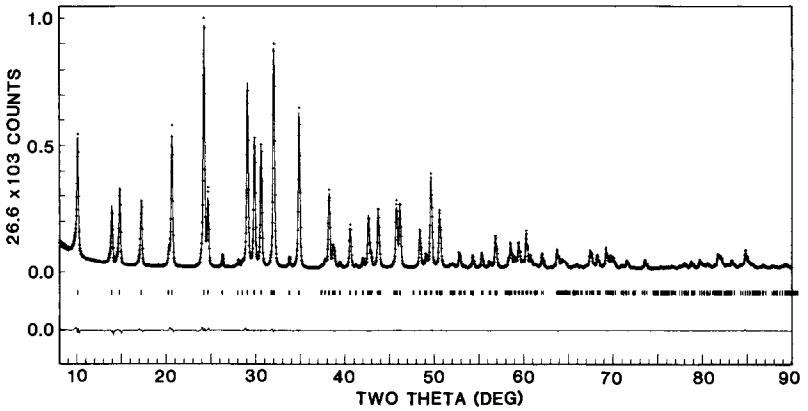

FIG. 1. Observed, calculated, and difference X-ray powder diffraction profile for $Cs_3Mo_2Cl_9$. The observed data are indicated by points and the calculated profile by the continuous line. The short vertical lines below the profile represent the positions of all possible Bragg reflections.

five refinements are given in Table II, together with calculated esd's. The latter are higher, by factors of 1.5 to 10, than the individual Rietveld esd's. The accuracy of the parameters obtained from the Rietveld refinements is indicated by a comparison of the average values in Table II with the corresponding reported values from the single-crystal refinement (*4*) (Table I). The coordinates agree within one combined esd and the cell parameters are within three combined esd's.

2. *Refinement of Structures in $P6_3/mmc$*

Single-crystal studies on the cesium compounds, $Cs_3Mo_2X_9$, X = Cl, Br (*4*), have previously shown that the correct space group is $P6_3/mmc$. Using this space group, we obtained satisfactory refinements of all compounds except the potassium salts (see below). For the alkali–metal compounds, the reported coordinates for $Cs_3Mo_2Cl_9$ (*4*) were used to initiate the Rietveld refinements. In the case of the alkylammonium salts, the maintaining of a relatively constant $(M_2X_9)^{3-}$ geometry in a much larger cell meant that the coordinates for the halogens could not be simply transferred from those of the alkali–metal compounds. Initial coordinates for Mo, N, and X were estimated geometrically from packing considerations. The positions of the carbon atoms were located in difference Fourier maps. They were assigned a group thermal vibration parameter and included in the refinement. However, in the presence of the heavy molybdenum and halogen X-ray scatterers, the contributions of the carbon atoms to the refinement were very low and the resulting refined coordinates reported in Table III give unrealistic C–N and C–C distances. The problem is accentuated for the Me_4N group located in the plane of the bridging halogens at $z = \frac{1}{4}$. This is a mirror plane in $P6_3/mmc$ and the Me_4N is disordered by reflection across the mirror, as reported for the related linear chain compound, $(Me_4N)MnCl_3$ (*16*).

The final refined unit cell parameters and atomic coordinates, as well as the weighted profile and Bragg R factors, R_{wp} and R_B, are listed in Table III.

3. *Refinement of $K_3Mo_2X_9$, X = Cl, Br*

The powder patterns for the potassium salts contain peaks of the type $(hh - \overline{2h}l)$ with $l = 2n + 1$, which violate the extinction conditions for $P6_3/mmc$.

TABLE III

RIETVELD REFINEMENT RESULTS FOR $A_3Mo_2X_9$ AND $Cs_3W_2Cl_9$ IN $P6_3/mmc$

	A = NH_4 X = Cl	Rb Cl	Me_4N Cl	Rb Br	Cs Br	Me_4N Br	Cs I	Cs W_2Cl_9
a (Å)	7.1351(2)	7.1622(3)	9.2374(7)	7.5217(6)	7.6296(5)	9.5093(9)	8.137(1)	7.3840(5)
c (Å)	16.9926(7)	17.015(1)	20.459(1)	17.930(2)	18.365(2)	21.366(2)	19.619(4)	17.093(1)
z (Mo)	0.8265(1)	0.8261(1)	0.8179(2)	0.8262(3)	0.8278(3)	0.8231(3)	0.8283(6)	0.8231(2)
z (A(2))	0.0692(8)	0.0723(2)	0.082(1)	0.0733(4)	0.0753(3)	0.117(2)	0.0767(5)	0.0761(3)
x (X(1))	0.4966(4)	0.4962(3)	0.5383(5)	0.4956(3)	0.5006(4)	0.5356(4)	0.5053(7)	0.5021(8)
x (X(2))	0.8265(3)	0.8270(2)	0.7868(3)	0.8276(3)	0.8260(3)	0.7932(3)	0.8296(7)	0.8236(7)
z (X(2))	0.0935(2)	0.0938(2)	0.1149(3)	0.0927(1)	0.0930(2)	0.1102(2)	0.0924(2)	0.0991(5)
R_{wp} (%)	9.74	5.81	9.57	7.06	6.49	9.69	6.52	9.43
R_B (%)	3.98	1.87	3.84	1.92	2.47	5.26	1.58	3.22

Methyl carbon refined coordinates for $(Me_4N)_3Mo_2X_9$:		X = Cl	X = Br
	C_{11} (0 0 z)	z = 0.171(3)	0.159(4)
	C_{12} (x 2x z)	x = 0.084(1)	0.091(4)
		z = 0.227(2)	0.223(3)
	C_{21} ($\frac{1}{3}$ $\frac{2}{3}$ z)	z = 0.143(2)	0.160(2)
	C_{22} (x 2x z)	x = 0.251(1)	0.263(1)
		z = 0.067(1)	0.041(1)

We have previously carried out a single-crystal structure analysis for $K_3Mo_2Cl_9$ (*6*) which confirmed that the space group was $P6_3/m$, as reported for the corresponding tungsten compound (*2*). The Rietveld refinement results for $K_3Mo_2Cl_9$ in $P6_3/m$ are compared with the (previously unpublished) results of the single-crystal refinement in Table IV. The coordinates agree within one combined esd and the cell parameters are within three combined esd's. The powder sample contained a minor amount of KCl and this was included as a second phase in the Rietveld refinement.

The X-ray powder profile data for the bromide compound, $K_3Mo_2Br_9$, was also refined in $P6_3/m$, and the results are included in Table IV. The higher weighted profile R factor is a consequence of poorer fitting to narrow peaks for this highly crystalline phase (FWHM at 40°, 2θ = 0.14°; cf. $Cs_3Mo_2Cl_9$, run E in Table II), as well as the

TABLE IV

RIETVELD REFINEMENT RESULTS FOR $K_3Mo_2X_9$ IN $P6_3/m$

	$K_3Mo_2Cl_9$		
	Rietveld ref.	Single crystal	$K_3Mo_2Br_9$
a (Å)	7.0989(3)	7.115(5)	7.4808(3)
c (Å)	16.623(1)	16.63(1)	17.5678(9)
z (Mo)	0.3259(3)	0.3261(4)	0.3233(3)
z (K(2))	0.5677(7)	0.5694(11)	0.5648(9)
x (X(1))	0.459(2)	0.462(8)	0.4578(9)
y (X(1))	0.446(2)	0.451(3)	0.4451(9)
x (X(2))	0.137(1)	0.129(8)	0.1257(7)
y (X(2))	0.349(1)	0.346(3)	0.3458(7)
z (X(2))	0.4983(4)	0.4075(12)	0.4066(2)
R_{wp} (%)	10.91		13.20
R_B (%)	2.79		4.11

presence of a minor amount of a second phase that could not be identified.

4. Structure Systematics in $A_3M_2X_9$

For A and X atoms of similar size, the structure of $A_3M_2X_9$ can be adequately described in terms of close packing of (0001) layers of composition AX_3, according to a six-layer stacking sequence *hcchcc* (*17*). The anion packing and the coordination of the M cations is illustrated in Fig. 2. The sites occupied by the two independent A cations are shown on the diagram. $A(1)$ lies in the plane of the $(M_2X_9)^{3-}$ *bridging* halogens, whereas $A(2)$ is displaced slightly from the plane of the $(M_2X_9)^{3-}$ *terminal* halogens. Both A cations are 12-coordinated but the geometry is different because of the change in layer-stacking sequence, from *h* (hexagonal) for Cs(1) (identical layers on either side) to *c* (cubic) for Cs(2) (cuboctahedral coordination) (*17*).

The effect of the relative sizes of A and X on their packing arrangement is shown in Fig. 3 for the *h* layer, containing the bridging halogens. In $Cs_3Mo_2Cl_9$, shown in Fig. 3a, the cesium and chloride ions are similar in size, with ionic radii 1.88 and 1.81 Å, respectively (*18*). These ions form an almost perfect hexagonal closest-packed layer. Figure 3b shows the effect of decreasing the size of the cation relative to the anion, for the case of $K_3Mo_2Cl_9$. The space group symmetry is lowered from $P6_3/mmc$ to $P6_3/m$ and the point group symmetry of the $(M_2X_9)^{3-}$ complex anion reduces from $\bar{6}m2$ to $\bar{6}$. This allows the triangular groupings of halogens in $(M_2X_9)^{3-}$ to rotate about the $\bar{6}$ axis towards the $A(1)$ anion sites, to reduce the $A(1)$–X bond lengths. The equatorial bonding geometry of $A(1)$ to $X(1)$ changes from a regular hexagon towards an edge-centered triangle, creating three short $A(1)$–$X(1)$ bonds.

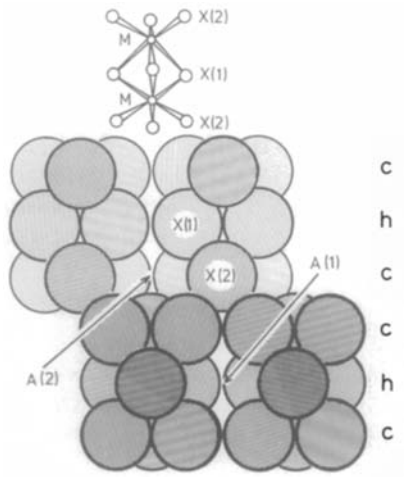

FIG. 2. Packing of anions in $A_3M_2X_9$, viewed along $[11\bar{2}0]$. Groups of anions are separated slightly to emphasize the $(M_2X_9)^{3-}$ complex anions. The $A(1)$ and $A(2)$ sites in the anion layers are indicated. The anion layer stacking sequence is shown. One $(M_2X_9)^{3-}$ anion is shown as a ball and spoke model to illustrate the M coordination and sharing of an octahedral face.

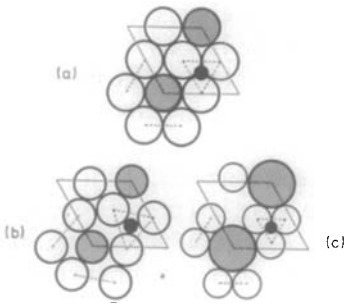

FIG. 3. The *h* layer of composition AX_3 in $A_3M_2X_9$, showing the effect of different A cation sizes. (a) $Cs_3Mo_2Cl_9$, (b) $K_3Mo_2Cl_9$, and (c) $(Me_4N)_3Mo_2Cl_9$. Shaded circles represent A, open circles are Cl, and solid circles are Mo, which lie above and below the layer. Triangular Cl_3 groupings associated with the $(Mo_2Cl_9)^{3-}$ complex anion are connected by dashed lines. The unit cell outline is shown, drawn to a common size to facilitate comparison.

The effect of increasing the size of the cation relative to the anion is illustrated in Fig. 3c for the case of $(Me_4N)_3Mo_2Cl_9$. The space group $P6_3/mmc$ is maintained but the increase in the x coordinate for $X(1)$ from the ideal value of $\frac{1}{2}$ results in a movement of the triangular clusters of bridging halogens away from each other. This opens up a large cavity to accommodate the $A(1)$ cation.

The effect of change of A cation on the geometry of the $(M_2X_9)^{3-}$ complex anion is shown by the changes in interatomic distances and angles in Table V. The results for the chloride and bromide series both show the same trends. With increase in A cation size there is a progressive increase in the M–M separation across the shared octahedral face with accompanying increases in the M–$X(1)$–M bridging angles, decreases in the $X(1)$–M–$X(1)$ angles, and decreases in the $X(1)$–$X(1)$ separations. In contrast, the geometry of the terminal halogens, $X(2)$, is hardly altered; the $X(2)$–$X(2)$ distances and $X(2)$–M–$X(2')$ angles do not vary significantly with change of A cation. The distances from the octahedral cations to the bridging and terminal halogens also remain essentially constant with average values of Mo–Cl(1) = 2.48(1) and Mo–Cl(2) = 2.40(2) Å for the series of chlorides. The corresponding average values for the bromide series are 2.63(2) and 2.54(1) Å, respectively. The longer bonds to the bridging halogens are expected on electrostatic grounds because $X(2)$ is coordinated to two M^{3+}, whereas $X(1)$ coordinates to only one M^{3+}. In this regard the results for $Cs_3Mo_2I_9$ are unexpected in that Mo–I(1) is slightly shorter than Mo–I(2) although within the associated esd's there is no significant difference between the two distances of 2.74(1) and 2.77(1) Å, respectively. An interesting feature of the iodide is the close approach to regular octahedral symmetry of the $(MoI_6)^{3-}$ octahedra. In addition to the almost equal Mo–I bond lengths, the I(1)–I(1) and I(2)–I(2) distances agree within the associated esd's, as do the $X(1)$–Mo–$X(1')$ and $X(2)$–Mo–$X(2')$ angles. The only distortion is a slight compression of the octahedra along z to accommodate the packing of Cs^+, which is smaller than I^-. Thus the geometry of the $(MoI_6)^{3-}$ octahedra is essentially that of an isolated octahedra and is not noticeably altered by face-sharing, as occurs for the chlorides and bromides.

The sequence of AX_3 and M layers along c is c-M-h-M-c-c-M-h-M-c. The cations thus occupy octahedral sites between h and c layers and share a common octahedral face across h layers. There are no occupied octahedral sites between pairs of c layers. The h and c layers are held tightly together by covalent M–X bonds and direct M–M bonding, whereas the pairs of c layers are held together only by relatively weak A–X bonds. The change of A cation size is accommodated along c almost exclusively by a change in the separation of the c layers. This is shown by the results for layer separations in Table VI. For the chloride series, from the K to the Me_4N salt, there is an increase in the c–c layer separation of 1.65 Å, whereas the c–h layer separation increases by only 0.13 Å. This latter increase is taken up exclusively in the separation of M from the plane of bridging halogens, i.e., M–h, shown in the third column of Table VI. The distance from M to the plane of terminal halogens, M–c, remains constant with change of A cation. The same observations apply to the bromide series. This constant M–c separation, together with unchanging $X(2)$–M–$X(2')$ angles, is reflected in an almost constant value of M–$X(2)$, which is 2.40(2) Å for the chlorides. This corresponds to the shortest Mo–Cl distance of 2.40(3) Å in the totally bridged compound α-$MoCl_3$ (*19*), and the Mo-terminal Cl distance of 2.38(1) Å in the $[Mo_2Cl_8]^{3-}$ anion (*20*).

The above results suggest that the observed increase of the M–M separation with increasing A cation size is due to the balance of three main factors: strong M–M bonding which draws the M atoms together, separation of the h and c layers due to increasing size of A, and strong covalent M–$X(2)$ bonds which maintain a constant M–c separation. The combination of the latter two factors results in increasing separation of M–M which acts against the M–M bonding and produces a net increase in

TABLE V

INTERATOMIC DISTANCES AND ANGLES FOR $A_3M_2X_9$[a]

A	*M*	*X*	*M*–*X*(1)	*M*–*X*(2)	*X*(1)–*X*(1′)[b]	*X*(2)–*X*(2′)[b]	*X*(1)–*X*(2)[c]
K	Mo	Cl	2.50(1)	2.400(7)	3.742(2)	3.41(1)	3.37(1)
NH_4	Mo	Cl	2.471(4)	2.398(4)	3.640(9)	3.421(6)	3.353(4)
Rb	Mo	Cl	2.480(3)	2.411(3)	3.663(6)	3.445(5)	3.360(3)
Cs	Mo	Cl	2.49(2)[d]	2.41(3)	3.64(4)	3.44(6)	3.39(2)
Me_4N	Mo	Cl	2.480(7)	2.363(6)	3.56(1)	3.329(8)	3.407(8)
K	Mo	Br	2.611(8)	2.567(5)	3.93(2)	3.652(7)	3.510(6)
Rb	Mo	Br	2.614(4)	2.551(4)	3.860(7)	3.630(7)	3.556(4)
Cs	Mo	Br	2.618(5)	2.559(4)	3.801(8)	3.647(6)	3.597(4)
Me_4N	Mo	Br	2.664(7)	2.525(6)	3.74(1)	3.610(9)	3.664(6)
Cs	Mo	I	2.74(1)	2.77(1)	3.94(2)	3.98(2)	3.845(8)
Cs	W	Cl	2.448(9)	2.407(9)	3.299(8)	3.47(2)	3.30(1)

A	*M*	*X*	*A*(1)–*X*(1)[b]	*A*(1)–*X*(2)[c]	*A*(2)–*X*(1)[c]	*A*(2)–*X*(2)[b]	*A*(2)–*X*(2)[c]
K	Mo	Cl	3.213(8)	3.402(6)	3.63(1)	3.30(1)	3.31(1)
NH_4	Mo	Cl	3.568(4)	3.416(4)	3.68(1)	3.40(1)	3.594(4)
Rb	Mo	Cl	3.581(3)	3.416(3)	3.637(3)	3.455(3)	3.600(2)
Cs	Mo	Cl	3.66(2)	3.51(3)	3.74(1)	3.58(3)	3.69(3)
Me_4N	Mo	Cl	4.659(4)	4.390(5)	4.75(1)	4.46(2)	4.726(5)
K	Mo	Br	3.378(5)	3.565(4)	3.87(2)	3.425(6)	3.49(1)
Rb	Mo	Br	3.761(4)	3.606(3)	3.809(6)	3.640(6)	3.778(3)
Cs	Mo	Br	3.815(4)	3.687(3)	3.895(5)	3.741(5)	3.830(3)
Me_4N	Mo	Br	4.791(5)	4.530(5)	4.38(3)	4.802(5)	4.802(4)
Cs	Mo	I	4.069(8)	3.915(7)	4.18(1)	4.03(1)	4.080(8)
Cs	W	Cl	3.692(9)	3.426(9)	3.673(7)	3.61(1)	3.715(7)

			Angles (°)				
A	*M*	*X*	*M*–*M*	*M*–*X*(1)–*M*	*X*(1)–*M*–*X*(1′)	*X*(2)–*M*–*X*(2′)	*X*(1)–*M*–*X*(2)
K	Mo	Cl	2.524(8)	60.6(4)	96.8(2)	90.6(2)	85.4(3)
NH_4	Mo	Cl	2.600(3)	63.5(1)	94.9(1)	91.0(1)	87.0(1)
Rb	Mo	Cl	2.590(4)	63.0(1)	95.2(1)	91.2(1)	86.7(1)
Cs	Mo	Cl	2.67(1)	64.8(6)	94.0(4)	91.1(9)	87.4(7)
Me_4N	Mo	Cl	2.778(8)	68.1(3)	91.7(3)	89.6(2)	89.4(2)
K	Mo	Br	2.57(1)	59.1(3)	97.8(2)	90.7(2)	85.9(2)
Rb	Mo	Br	2.731(9)	63.0(2)	95.2(1)	90.7(2)	87.0(1)
Cs	Mo	Br	2.86(1)	66.1(2)	93.1(1)	90.9(2)	88.0(1)
Me_4N	Mo	Br	3.12(1)	71.8(3)	89.1(2)	91.3(2)	89.8(1)
Cs	Mo	I	3.07(2)	68.1(5)	91.7(3)	91.6(3)	88.3(2)
Cs	W	Cl	2.500(7)	61.4(3)	96.2(2)	92.4(3)	85.6(3)

[a] *X*–*X* distances and associated angles are for *X* within the same $(M_2X_9)^{3-}$.

[b] Both atoms in the same (0001) layer.

[c] Distances between atoms in adjacent (0001) layers.

[d] esd's for $Cs_3Mo_2Cl_9$ from averaging of results for five independent Rietveld refinements. Other esd's derived from Rietveld esd's on coordinates.

TABLE VI

LAYER SEPARATIONS ALONG c IN $A_3M_2X_9$

A	M	X	c–h	c–c	M–h	M–c
K	Mo	Cl	2.63	3.05	1.26	1.37
NH_4	Mo	Cl	2.66	3.18	1.30	1.36
Rb	Mo	Cl	2.66	3.19	1.29	1.36
Cs	Mo	Cl	2.70	3.36	1.33	1.36
Me_4N	Mo	Cl	2.76	4.70	1.39	1.37
K	Mo	Br	2.75	3.28	1.29	1.46
Rb	Mo	Br	2.82	3.32	1.37	1.45
Cs	Mo	Br	2.88	3.42	1.43	1.45
Me_4N	Mo	Br	2.99	4.71	1.56	1.43
Cs	Mo	I	3.09	3.62	1.54	1.55
Cs	W	Cl	2.58	3.39	1.25	1.33
K	W	Cl[a]	2.55	3.00	1.21	1.35

[a] From Ref. (*2*).

M–M with increasing A. In the corresponding tungsten compounds, the M–M bonding is stronger and the resistance against the M–M lengthening factors is greater. The increase in W–W from the K to the Cs salt is only 0.09 Å, compared with an increase in Mo–Mo of 0.15 Å for the corresponding molybdenum compounds.

The results in Table VI show that in both the chloride and bromide series, there is a net attraction of the molybdenum atoms towards one another, from the octahedral centers, for cations up to Cs. For the Me_4N salts, the molybdenum atoms are displaced outwards from the octahedra centers, the displacement being greater for the bromide. As mentioned above, the molybdenum atoms are centrally located in the octahedra in $Cs_3Mo_2I_9$.

For the chloride series, the Mo–Mo separations obtained from the Rietveld refinements agree to within 0.01 Å with the values we previously reported, based on using a fixed Mo z coordinate (*1*). However, the refined Mo–Mo for the Me_4N salt, 2.778(8) Å, is markedly shorter than the value previously estimated of 3.13 Å, and this will have a marked effect on the relationship between the magnetic exchange integral, $-J$, and the Mo–Mo separation. A detailed analysis of the magnetic interactions in terms of the refined $(M_2X_9)^{3-}$ geometries will be presented elsewhere.

References

1. I. E. GREY AND P. W. SMITH, *Austral. J. Chem.* **24,** 73 (1971).
2. W. H. WATSON AND J. WASER, *Acta Crystallogr.* **11,** 689 (1958).
3. G. J. WESSEL AND D. J. W. IJDO, *Acta Crystallogr.* **10,** 466 (1957).
4. R. SAILLANT, R. B. JACKSON, W. E. STREIB, K. FOLTING, AND R. A. D. WENTWORTH, *Inorg. Chem.* **10,** 1453 (1971).
5. R. STRANGER, Ph.D. thesis, University of Tasmania, Hobart (1986).
6. I. E. GREY, Ph.D. thesis, University of Tasmania, Hobart (1969).
7. M. YU. SUBBOTIN AND L. A. ASLANOV, *Russian J. Inorg. Chem.* **30,** 816 (1985).
8. H. M. RIETVELD, *J. Appl. Crystallogr.* **2,** 64 (1969).
9. I. E. GREY AND P. W. SMITH, *Austral. J. Chem.* **22,** 121 (1969).
10. I. E. GREY AND P. W. SMITH, *Austral. J. Chem.* **22,** 1627 (1969).
11. D. B. WILES AND R. A. YOUNG, *J. Appl. Crystallogr.* **14,** 149 (1981).
12. R. J. HILL AND C. J. HOWARD, *J. Appl. Crystallogr.* **18,** 173 (1985).
13. G. CAGLIOTTI, A. PAOLETTI, AND F. P. RICCI, *Nucl. Instrum.* **3,** 223 (1958).
14. R. J. HILL AND I. C. MADSEN, *J. Electrochem. Soc.* **131,** 1486 (1984).
15. "International Tables for X-Ray Crystallography," Vol. IV, Kynoch Press, Birmingham, England (1974).
16. B. MOROSI AND E. J. GRAEBER. *Acta Crystallogr.* **23,** 766 (1967).
17. I. E. GREY, I. C. MADSEN, S. E. BUTLER, P. W. SMITH, AND R. S. STRANGER, *Acta Crystallogr., Sect. C* **42** (1986).
18. R. D. SHANNON AND C. T. PREWITT, *Acta Crystallogr., Sect. B* **25,** 925 (1969).
19. H. SCHAFER, H. G. SCHNERING, J. TILLACK, F. KUHNEN, H. WÖHRLE, AND H. BAUMAN, *Z. Anorg. Allg. Chem.* **353,** 281 (1967).
20. M. J. BENNETT, J. V. BRENCIC, AND F. A. COTTON, *Inorg. Chem.* **8,** 1060 (1969).